# Comparison of Subspace and ARX Models of a Waveguide's Terahertz Transient Response After Optimal Wavelet Filtering

Sillas Hadjiloucas, *Member, IEEE*, Roberto K. H. Galvão, Victor M. Becerra, *Senior Member, IEEE*, John W. Bowen, Rainer Martini, Martin Brucherseifer, Harm P. M. Pellemans, Peter Haring Bolívar, *Member, IEEE*, Heinrich Kurz, and J. Martyn Chamberlain

***Abstract*—A quasi-optical deembedding technique for characterizing waveguides is demonstrated using wide-band time-resolved terahertz spectroscopy. A transfer function representation is adopted for the description of the signal in the input and output port of the waveguides. The time-domain responses were discretized and the waveguide transfer function was obtained through a parametric approach in the $z$-domain after describing the system with an AutoRegressive with eXogenous input (ARX), as well as with a state-space model. Prior to the identification procedure, filtering was performed in the wavelet domain to minimize both signal distortion, as well as the noise propagating in the ARX and subspace models. The optimal filtering procedure used in the wavelet domain for the recorded time-domain signatures is described in detail. The effect of filtering prior to the identification procedures is elucidated with the aid of pole-zero diagrams. Models derived from measurements of terahertz transients in a precision WR-8 waveguide adjustable short are presented.**

***Index Terms*—Identification algorithms, multimode waveguide characterization, signal processing, terahertz spectroscopy.**

## I. Introduction

THIS PAPER discusses quasi-optical broad-band measurements of the scattering parameters, attenuation coefficients, and characteristic impedances of waveguide components at submillimeter-wave frequencies performed using a terahertz-transient spectrometer.

Although there are inherent advantages in broad-band measurements using very short terahertz pulses as the individual reflection signatures of the device-under-test are in the time domain and, therefore, can be directly isolated and gated out, the frequency bands within which the device-under-test exhibits monomode operation must be identified. A further difficulty that arises is that most of the power output from the wide-band pulsed source occurs at frequencies (e.g., 1–3 THz) where waveguides designed for lower frequencies can support a number of modes. At frequencies where multimoded propagation can occur, a meaningful analysis is only possible if the extent to which each waveguide mode has been excited is known. Finally, the power output of the source over the single-moded bandwidth of the waveguide is often rather low, leading to a poor signal-to-noise ratio in each frequency bin of the complex insertion loss function.

In this paper, the problems associated with poor signal-to-noise ratio and multimoded propagation are addressed by placing the waveguide characterization problem in a system identification framework. We introduce autoregressive and state-space models as efficient modeling tools of linear processes such as energy dissipation in a waveguide test piece. These tools, however, require low-noise data sets, which might not be realizable within practical integration time scales. Wavelet pre-filtering is well suited to the denoising of the nonstationary data sets obtained in terahertz transient spectrometry [1]–[3]. Since the commonly used wavelets such as the $db4$ family are not necessarily optimal in describing an experimental data set, we introduce a process for tailoring the wavelet transform to the signal to be analyzed in order to maximize the amount of energy in the wavelet coefficients kept in the filtering process. The algorithm is then used to process terahertz transient reflection signatures from a WR-8 adjustable waveguide short. The identification models provide the weights and attenuation for each mode propagating in the structure. Pole-zero diagrams are used to show the effect of filtering on the calculated mode parameters.

## II. Experimental Setup

The experimental setup for generating and detecting terahertz radiation is shown in Fig. 1(a). A mode-locked Ti:sapphire

Manuscript received April 30, 2003; revised June 11, 2004. This work was supported in part by the European Community Training and Mobility of Researchers under Grant FMRX-CT96-0092, by the Fundação de Amparo à Pesquisa do Estado de São Paulo under Grant 00/09390-6, by the Programa de Apoio a Núcleos de Excelência/Conselho Nacional de Desenvolvimento Científico e Tecnológico under Grant 015/98, and by the Conselho Nacional de Desenvolvimento Científico e Tecnológico under a Research Fellowship.

S. Hadjiloucas, V. M. Becerra, and J. W. Bowen are with the Department of Cybernetics, The University of Reading, Reading RG6 6AY, U.K. (e-mail: cybsh@cyber.rdg.ac.uk).

R. K. H. Galvão is with the Divisão de Engenharia Eletrônica, Instituto Tecnológico de Aeronáutica, São José dos Campos-SP, Brazil (e-mail: kawakami@ele.ita.br).

R. Martini is with the Physics and Engineering Physics Department, Stevens Institute of Technology, Hoboken, NJ 07030 USA (e-mail: rmartini@stevens.edu).

M. Brucherseifer is with the Applied Sensors Laboratory, School of Chemistry and Biochemistry, Georgia Institute of Technology, Atlanta, GA USA 30332 (e-mail: martin@brucherseifer.com).

H. P. M. Pellemans is with ASML Holding N.V., Veldhoven, 5504 DR Veldhoven, The Netherlands (e-mail: harm@pellemans.com).

P. Haring Bolívar and H. Kurz are with the Institut für Halbleitertechnik, Rhejnisch Westfalische Technische Hochschule Aachen, 52056 Aachen, Germany (e-mail: haring@iht.rwth-aachen.de).

J. M. Chamberlain is with Grey College, University of Durham, Durham DH1 3LG, U.K. (e-mail: martyn.chamberlain@durham.ac.uk).

Digital Object Identifier 10.1109/TMTT.2004.835983

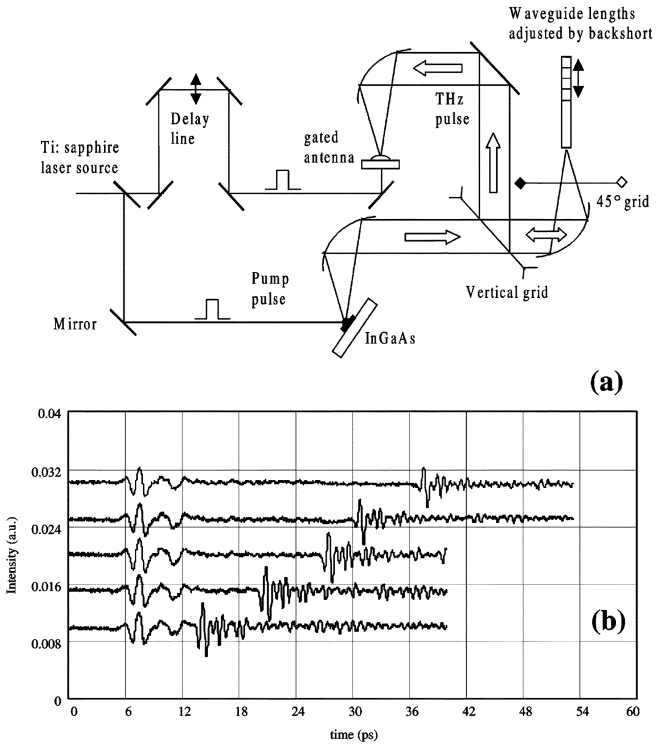


Fig. 1. (a) Experimental setup for waveguide characterization. (b) Time-domain reflection signatures for five shorted WR-8 waveguides differing in length by 1 mm. The signals are vertically offset for better visualization.

laser producing optical pulses with durations of ∼140 fs is used to resonantly excite the lowest interband transitions of an InGaAs emitter, which is located at the focal point of a parabolic reflector [4]–[6]. The optical pulse generates an electron–hole plasma and the accelerated carriers generate a pulse of terahertz radiation that is horizontally polarized along the direction of the surface field of the InGaAs emitter. Terahertz pulses emitted by the photoconductive element are transmitted through a vertical grid and the propagating terahertz beam, which has a Gaussian transverse amplitude distribution, is focused by the second parabolic mirror to feed at normal incidence, in a co-polar manner, the open port of the waveguide under test. The optics are designed to give a frequency-independent beam waist at the test port. The effective beam-waist size and location to optimally feed the waveguide will change in frequency, but will be independent of the location of the short in the waveguide. Thus, at any given frequency, the coupling coefficient between the beam and waveguide remains constant regardless of the position of the short. Upon 180° reflection at the back short, the modified terahertz pulse exits the waveguide and is focused to a time-gated ion-implanted silicon-on-sapphire photoconductive dipole antenna [7].

A sequence of measurements was performed on a commercially available precision WR-8 waveguide adjustable short. The time-domain interferograms corresponding to five different positions of the backshort at 1-mm spacings are shown in Fig. 1(b).

Maintaining the location of the waveguide relative to the beam and using an adjustable short to provide different test waveguide lengths ensured that a constant degree of coupling

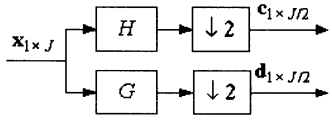


Fig. 2. Two-channel filter bank. Blocks $H$ and $G$ represent a low-pass and a high-pass filter, respectively and $\downarrow$ 2 denotes the operation of dyadic downsampling. The decomposition can be carried out in more resolution levels by successively splitting the low-pass channel.

was maintained between the terahertz beam and the test piece throughout the measurement sequence. The terahertz pulse produced by the photoconductive antenna has frequency components up to 3 THz.

## III. Wavelet Pre-Filtering

### A. Filter Bank Formulation of the Discrete Wavelet Transform

Prior to the identification procedures, the time-domain signatures reflected by the short at the end of each waveguide length were detrended by subtracting the mean. Such a detrending was performed to avoid the need to include an offset term in the identification model [8]. Wavelet filtering was performed because it is known to produce better results than conventional filters when the signal is nonstationary [9], [10]. The wavelet filtering process was performed using a filter bank formulation of the wavelet transform [11]. Each time-domain signature was represented by a data vector $\mathbf{x}$ of length $J$, where the $n$th element of $\mathbf{x}$, denoted by $x_n$, represents the measured signal at the $n$th sampling instant. The filter bank transform can be regarded as a change in variables from $\Re^J$ to $\Re^J$ performed according to the following operation:

$$t_k = \sum_{n=0}^{J-1} x_n v_k(n), \qquad k = 0, \ldots, J-1 \tag{1}$$

where $t_k$ is a transformed variable and $v_k(n) \in \Re$ is a transform weight. It proves convenient to write the transform in matrix form as

$$\mathbf{t}_{1\times J} = \mathbf{x}_{1\times J}\mathbf{V}_{J\times J} \tag{2}$$

where $\mathbf{x} = [x_0 x_1 \ldots x_{J-1}]$ is the row vector of original variables, $\mathbf{t}$ is the row vector of new (transformed) variables, and $\mathbf{V}$ is the matrix of weights. Choosing $\mathbf{V}$ to be unitary (i.e., $\mathbf{V}^T\mathbf{V} = \mathbf{I}$), the transform is said to be orthogonal and it, therefore, consists of a simple rotation in the coordinate axes (with the new axes directions determined by the columns of $\mathbf{V}$). As described in the wavelet literature [12]–[14], the discrete wavelet transform can be calculated in a fast manner by using a finite impulse response (FIR) filter bank structure of the form depicted in Fig. 2. It is worth noting that general $M$-channel FIR filter bank decompositions could also be employed in this context [15], but the scope of this paper will be restricted to two-channel filter banks, as in Fig. 2.

In this filter bank, the low-pass filtering result undergoes successive filtering iterations with the number of iterations $k$ chosen by the analyst. The final result of the decomposition of data vector $\mathbf{x}$ is a vector resulting from the concatenation of row

TABLE I
CONVOLUTION PROCEDURE FOR LOW-PASS FILTERING SHOWING RESULTS BEFORE AND AFTER DYADIC DOWNSAMPLING

| $x_0$ | $x_1$ | $\cdots$ | $x_{2N-1}$ | $x_{2N}$ | $\cdots$ | $x_{J-1}$ | $x_0$ | $x_1$ | ... | $x_{2N-2}$ | Before | After |
|---|---|---|---|---|---|---|---|---|---|---|---|---|
| $h_{2N-1}$ | $h_{2N-2}$ | $\cdots$ | $h_0$ | | | | $\cdots$ | | | | $c_0'$ | |
| | $h_{2N-1}$ | $\cdots$ | $h_1$ | $h_0$ | | | $\cdots$ | | | | $c_1'$ | $c_0$ |
| | | $\cdots$ | | $\vdots$ | | | | $\cdots$ | | | $\vdots$ | $\vdots$ |
| | | | | | | $h_{2N-1}$ | $h_{2N-2}$ | $h_{2N-3}$ | $\cdots$ | | $c_{J-2}'$ | |
| | | | | | | | $h_{2N-1}$ | $h_{2N-2}$ | $\cdots$ | $h_0$ | $c_{J-1}'$ | $c_{J/2-1}$ |

vectors $\mathbf{c}(k)$ and $\mathbf{d}(k)$ (termed approximation and detail coefficients at the $k$th scale level, respectively) in the following manner:

$$\mathbf{t} = \big[\mathbf{c}(k)|\mathbf{d}(k)|\mathbf{d}(k-1)|\ldots|\mathbf{d}(1)\big]. \tag{3}$$

with coefficients in larger scales (e.g., $\mathbf{d}(k), \mathbf{d}(k-1), \mathbf{d}(k-2), \ldots$) associated with broad features in the data vector, and coefficients in smaller scales (e.g., $\mathbf{d}(1), \mathbf{d}(2), \mathbf{d}(3), \ldots$) associated with narrower features such as sharp peaks.

Let $\{h_0, h_1, \ldots, h_{2N-1}\}$ and $\{g_0, g_1, \ldots, g_{2N-1}\}$ be the impulse responses of the low-pass and high-pass filters, respectively. Assuming that filtering is carried out by circular convolution, the procedure for generating the approximation coefficients from the data vector $\mathbf{x}$ is illustrated in Table I. The convolution consists of flipping the filtering sequence and moving it alongside the data vector. For each position of the filtering sequence with respect to the data vector, the scalar product of the two is calculated (with missing points in the filtering sequence replaced with zeros). For instance, if $N = 2$, the third row in Table I shows that $c_1' = x_1h_3 + x_2h_2 + x_3h_1 + x_4h_0$. Dyadic downsampling is then performed to $c_{2i}'$ to generate coefficients $c_i$. The detail coefficients $d_i$ are obtained in a similar manner by using the high-pass filtering sequence.

If the approximation $\mathbf{c}$ and detail $\mathbf{d}$ coefficients are stacked in vector $\mathbf{t} = [\mathbf{c}\,|\,\mathbf{d}]$, the wavelet transform can be expressed in the matrix form (2) with the transformation matrix given by (4), shown at the bottom of this page.

A requirement for the transform to be orthogonal (i.e., $\mathbf{V}^T\mathbf{V} = \mathbf{I}$) is that the sum of the squares of each column must be equal to one and the scalar product of different columns must be equal to zero. Therefore, for a filter bank that utilizes low-pass and high-pass filters, the following conditions ensure orthogonality of the transform so that no information is lost in the decomposition process [11]

$$\sum_{n=0}^{2N-1-2l} h_n h_{n+2l} = \begin{cases} 1, & l = 0 \\ 0, & 0 < l < N \end{cases} \tag{5a}$$

$$g_n = (-1)^{n+1} h_{2N-1-n}, \quad n = 0, 1, \ldots, 2N-1. \tag{5b}$$

If the filtering sequences satisfy these conditions, the entire structure is termed a quadrature-mirror filter (QMF) bank [12]. A QMF bank is said to enjoy a perfect reconstruction (PR) property because $\mathbf{x}$ can be reconstructed from $\mathbf{t}$, which means that there is no loss of information in the decomposition process. In fact, from the relation $\mathbf{t} = \mathbf{x}\mathbf{V}$, it follows that $\mathbf{t}\mathbf{V}^{\mathrm{T}} = \mathbf{x}\mathbf{V}\mathbf{V}^{\mathrm{T}}$ and $\mathbf{x} = \mathbf{t}\mathbf{V}^{\mathrm{T}}$, due to the orthogonality of the transform. At this point, it should be noticed that other nonorthogonal transforms can also enjoy a PR property, provided that they are associated to a nonsingular matrix $\mathbf{V}$. However, the analysis in this paper will be restricted to orthogonal transforms.

Filtering in the wavelet domain consists of replacing some of the elements of $\mathbf{t}$ by zero so that a new vector $\bar{\mathbf{t}}$ is produced and then applying the inverse transform.

### *B. Filtering Using Adaptively Chosen Wavelets*

One limitation of the procedure described for the filtering of the time-domain signatures in the wavelet domain is that the wavelets must be chosen *a priori* and are not adapted to optimally describe the experimental data set. Optimizing the transform to maximize its compression ability and, therefore, its efficiency is normally achieved by optimizing the QMF bank. The QMF bank can be described by a set of parameters that can be adjusted by any algorithm for unconstrained optimization to maximize the compression ability of the transform.

The parametrization of PR FIR filter banks proposed by Vaidyanathan as adapted by Sherlock and Monro [13] to parametrize orthonormal wavelets of arbitrary compact support

$$\mathbf{V} = \left[\begin{array}{ccccc|ccccc} 0 & 0 & \cdots & h_{2N-4} & h_{2N-2} & 0 & 0 & \cdots & g_{2N-4} & g_{2N-2} \\ h_{2N-1} & 0 & \cdots & h_{2N-5} & h_{2N-3} & g_{2N-1} & 0 & \cdots & g_{2N-5} & g_{2N-3} \\ h_{2N-2} & 0 & \cdots & h_{2N-6} & h_{2N-4} & g_{2N-2} & 0 & \cdots & g_{2N-6} & g_{2N-4} \\ h_{2N-3} & h_{2N-1} & \cdots & h_{2N-7} & h_{2N-5} & g_{2N-3} & g_{2N-1} & \cdots & g_{2N-7} & g_{2N-5} \\ \vdots & \vdots & \vdots & \vdots & \vdots & \vdots & \vdots & \vdots & \vdots & \vdots \\ h_0 & h_2 & \cdots & 0 & 0 & g_0 & g_2 & \cdots & 0 & 0 \\ 0 & h_1 & \cdots & 0 & 0 & 0 & g_1 & \cdots & 0 & 0 \\ 0 & h_0 & \cdots & 0 & 0 & 0 & g_0 & \cdots & 0 & 0 \\ \vdots & \vdots & \vdots & \vdots & \vdots & \vdots & \vdots & \vdots & \vdots & \vdots \\ 0 & 0 & \cdots & h_{2N-2} & 0 & 0 & 0 & \cdots & g_{2N-2} & 0 \\ 0 & 0 & \cdots & h_{2N-3} & h_{2N-1} & 0 & 0 & \cdots & g_{2N-3} & g_{2N-1} \end{array}\right] \tag{4}$$

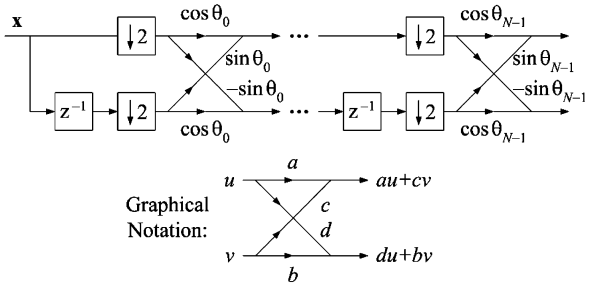


Fig. 3. Procedure for parameterizing wavelet filter banks by $N$ angles.

may be used for this purpose. For a filter bank of the form shown in Fig. 2 where the conditions in (5a) and (5b) are satisfied, the transfer function of the low-pass filter in the $z$-domain can be written as

$$H^{(N)}(z) = \sum_{n=0}^{2N-1} h_n^{(N)} z^{-n} = H_0^{(N)}\left(z^2\right) + z^{-1} H_1^{(N)}\left(z^2\right) \tag{6}$$

where superscript $(N)$ denotes that the filtering sequences have length $2N \cdot H_0^{(N)}(z)$ and $H_1^{(N)}(z)$, termed polyphasic components of $H^{(N)}(z)$, are given by

$$H_0^{(N)}(z) = \sum_{i=0}^{N-1} h_{2i}^{(N)} z^{-i} \tag{7a}$$

$$H_1^{(N)}(z) = \sum_{i=0}^{N-1} h_{2i+1}^{(N)} z^{-i}. \tag{7b}$$

Defining the polyphasic components $G_0^{(N)}(z)$ and $G_1^{(N)}(z)$ of the high-pass filter $G^{(N)}(z)$ in a similar manner, a matrix $F^{(N)}(z)$ may be defined as follows:

$$F^{(N)}(z) = \begin{bmatrix} H_0^{(N)}(z) & H_1^{(N)}(z) \\ G_0^{(N)}(z) & G_1^{(N)}(z) \end{bmatrix}. \tag{8}$$

It can be shown [11], [12] that $F^{(N)}(z)$ can be factorized as

$$F^{(N)}(z) = \begin{bmatrix} C_0 & S_0 \\ -S_0 & C_0 \end{bmatrix} \prod_{i=1}^{N-1} \begin{bmatrix} 1 & 0 \\ 0 & z^{-1} \end{bmatrix} \begin{bmatrix} C_i & S_i \\ -S_i & C_i \end{bmatrix} \tag{9}$$

where each pair of parameters $(C_i, S_i)$ are related to a common angular parameter $\theta_i$ as $C_i = \cos(\theta_i)$ and $S_i = \sin(\theta_i), i = 0, 1, \ldots, N-1$. It follows that the filters can be completely parameterized by $N$ angles $\theta_0, \theta_1, \ldots, \theta_{N-1}$, which can assume any value in the set of real numbers, as shown in Fig. 3.

The weights of the low-pass filter can be easily recovered from a set of angles $\{\theta_i\}$ by using the following recursive formula [11], [12]:

$$F^{(k+1)}(z) = F^{(k)}(z) \cdot \begin{bmatrix} 1 & 0 \\ 0 & z^{-1} \end{bmatrix} \begin{bmatrix} C_k & S_k \\ -S_k & C_k \end{bmatrix} \tag{10}$$

for $k = 1, 2, \ldots, N-1$ with

$$F^{(1)}(z) = \begin{bmatrix} C_0 & S_0 \\ -S_0 & C_0 \end{bmatrix}. \tag{11}$$

Equation (10) with the initial condition of (11) provide a way to obtain the weights $\{h_i^{(k+1)}\}$ for a filter of length $2(k+1)$ from the weights $\{h_i^{(k)}\}$ for a filter of length $2k$. To do that, one starts by writing, from (8) and (10)

$$H_0^{(k+1)}(z) = H_0^{(k)}(z) C_k - z^{-1} H_1^{(k)}(z) S_k, \quad k = 1, 2, \ldots, N-1 \tag{12a}$$

$$H_1^{(k+1)}(z) = H_0^{(k)}(z) S_k + z^{-1} H_1^{(k)}(z) C_k, \quad k = 1, 2, \ldots, N-1 \tag{12b}$$

with $H_0^{(1)}(z) = C_0$ and $H_1^{(1)}(z) = S_0$. A recursive formula for the generation of low-pass filter weights with even indexes $\{h_{2i}\}$ can then be stated by using the definitions in (7a) and (7b) to expand (12a) as

$$\overbrace{\sum_{i=0}^{k} h_{2i}^{(k+1)} z^{-i}}^{H_0^{(k+1)}(z)} = \overbrace{\left(\sum_{i=0}^{(k-1)} h_{2i}^{(k)} z^{-1}\right)}^{H_0^{(k)}(z)} C_k - z^{-1} \overbrace{\left(\sum_{i=0}^{(k-1)} h_{2i+1}^{(k)} z^{-1}\right)}^{H_1^{(k)}(z)} S_k \Rightarrow$$

$$\sum_{i=0}^{k} h_{2i}^{(k+1)} z^{-i} = C_k h_0^{(k)} + \sum_{i=1}^{k-1} \left(C_k h_{2i}^{(k)} - S_k h_{2i-1}^{(k)}\right) z^{-i} - S_k h_{2k-1}^{(k)} z^{-k} \tag{13}$$

for $k = 1, 2, \ldots, N-1$, with $h_0^{(1)} = C_0$ and $h_1^{(1)} = S_0$. From the identity of terms with the same power of $z$ in the last line of (13), it follows that

$$\begin{cases} h_0^{(k+1)} = C_k h_0^{(k)} \\ h_{2i}^{(k+1)} = C_k h_{2i}^{(k)} - S_k h_{2i-1}^{(k)}, & i = 1, 2, \ldots, k-1 \\ h_{2k}^{(k+1)} = -S_k h_{2k-1}^{(k)} \end{cases} \tag{14a}$$

for $k = 1, 2, \ldots, N-1$.

A similar formula can be stated for the low-pass filter weights with odd indexes by expanding (12b) as

$$\begin{cases} h_1^{(k+1)} = S_k h_0^{(k)} \\ h_{2i+1}^{(k+1)} = S_k h_{2i}^{(k)} + C_k h_{2i-1}^{(k)}, & i = 1, 2, \ldots, k-1 \\ h_{2k+1}^{(k+1)} = C_k h_{2k-1}^{(k)} \end{cases} \tag{14b}$$

for $k = 1, 2, \ldots, N-1$. After obtaining the low-pass filtering sequence, as explained above, the high-pass filtering sequence can be obtained by using (5b).

Condition (5a) states that the $2N$ weights $\{h_n\}$ of the low-pass filter are subject to $N$ restrictions. Thus, there are $N$ degrees of freedom that can be used to optimize the filter bank according to some performance criterion. It is worth noting that since the restrictions are nonlinear and may define a nonconvex search space, the optimization task is not trivial. We circumvent this difficulty by using the lattice structure for the filter bank, which is parameterized by $N$ angles $\{\theta_0, \theta_1, \ldots, \theta_{N-1}\}$ that can assume any real value, as shown in Fig. 3.

The problem then becomes one of unconstrained optimization in $\mathrm{R}^N$. The optimal filtering procedure employed in this study was aimed at maximizing the amount of energy in the wavelet coefficients kept in the thresholding process. The optimization consisted of maximizing an objective function $F(\theta) : \mathrm{R}^N \rightarrow \mathrm{R}$ defined as

$$F(\theta) = \sum_{k \in \mathrm{I}} p^2(k; \theta) \tag{15}$$

where $\theta$ is the vector of $N$ angles that parameterize the filter bank, as explained above, $p(k;\theta)$ is the $k$th wavelet coefficient resulting from the signal decomposition, and $\mathrm{I}$ is the index set of the coefficients kept in the thresholding process. It is worth noting that $\mathrm{I}$ is defined on the basis of the magnitude of the wavelet coefficients before the optimization. The flexible polyhedron algorithm available in the MATLAB Optimization Toolbox was employed to search for the optimum $\theta$ using the parameters associated with the $db4$ wavelet as a starting point. The optimization was carried out separately for each signal.

It is possible that the objective function (15) may have local maxima different from the global maximum. In that case, the flexible polyhedron algorithm will tend to converge to the closest local maximum. However, even if the global maximum is not attained, an improvement over the original wavelet transform may still be obtained.

For comparative purposes, a nonoptimized filtering procedure, where each time-domain signal $\mathbf{x}$ to be filtered was decomposed using a $db4$ wavelet filter bank with two resolution levels [16], was also performed. Hard thresholding was employed, with all wavelet coefficients with magnitude smaller than a certain fraction of the largest coefficient being replaced with zeros. The inverse transform was then applied to obtain the filtered signal shown in Fig. 4.

As can be seen from Fig. 4, a direct comparison between filtered and optimally filtered waveforms is almost impossible in the time-domain plots. Plotting, however, pole-zero diagrams after performing system identification for the terahertz-transient excited waveguide sections makes the effect of filtering more apparent.

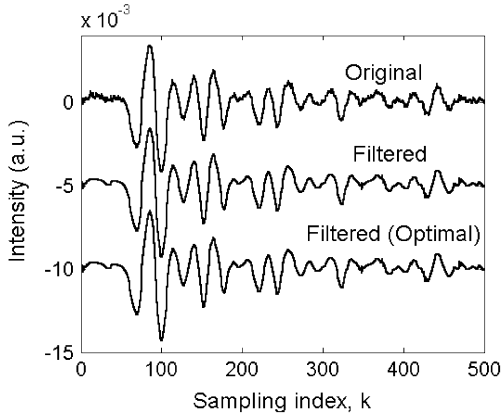


Fig. 4. Unfiltered, filtered, and optimally filtered time-domain responses for the 2-mm-long WR-8 waveguide section.

## IV. SYSTEM IDENTIFICATION

### A. ARX Model

This section describes the process of obtaining the frequency response of a waveguide test piece by identifying a parametric model from the reflection signatures for two different waveguide lengths. Let $u(t)$ and $y(t)$ be the reflection signatures for the shorter (length $Ld$, where $d$ is a length unit) and longer (length $(L+1)d$) waveguides, respectively. Ratioing the spectra $U(\omega)$ and $Y(\omega)$ yields the effective complex insertion loss function $H(\omega)$ for a unit length waveguide [17] that is given from $H(\omega) = Y(\omega)/U(\omega)$, where $H(\omega)$ can be regarded as the frequency response of a linear system, which produces an output $y(t)$ for an input $u(t)$.

Instead of using the ratioing procedure, which is very sensitive to measurement noise, system identification techniques can be employed to obtain the complex insertion loss. Since this approach is novel in the context of waveguide characterization, results from two different identification techniques will be presented to demonstrate this concept. Firstly, $H(\omega)$ can be obtained directly through a parametric approach [8], [18] in which the unit length waveguide is described by an AutoRegressive with eXogenous input (ARX) model of the form

$$\begin{aligned} y[\mathrm{k}] + a_1 y[\mathrm{k}-1] + \cdots + a_{n_a} y[\mathrm{k}-n_a] \\ = b_1 u[\mathrm{k}-n_\mathrm{k}] + b_2 u[\mathrm{k}-n_\mathrm{k}-1] + \cdots \\ + b_{n_b} u[\mathrm{k}-n_\mathrm{k}-n_b+1] + \varepsilon[\mathrm{k}] \end{aligned} \tag{16}$$

where $y[\mathrm{k}]$ is the response measured at time $\mathrm{k}T_s$ (sampling interval $T_s = 27$ femtoseconds), $\{a_1, \ldots, a_{n_a}, b_1, \ldots, b_{n_b}\}$ are model coefficients, $n_a$ is the number of poles (equivalent to the system order), $(n_b - 1)$ is the number of zeros, $n_\mathrm{k}$ is a pure time delay, and $\varepsilon[\mathrm{k}]$ is a residual. $H(\omega)$ can be discretized as a $z$-domain transfer function $H_d(z) = Y(z)/U(z)$

$$\begin{aligned} H_d(z) &= z^{-n_\mathrm{k}} \frac{b_1 + b_2 z^{-1} + \cdots b_{n_b} z^{-n_b+1}}{1 + a_1 z^{-1} + \cdots a_{n_a} z^{-n_a}} \\ &= z^{-n_\mathrm{k}} \frac{N(z)}{D(z)} = z^{-n_k} \sum_{i=1}^{n+m} w_i \frac{1 + f_i z^{-1}}{1 + c_{i1} z^{-1} + c_{i2} z^{-2}} \end{aligned} \tag{17}$$

by making $z = \exp(j\omega T_s)$. The roots of $D(z)$ (poles of $H_d(z)$) are associated with the $\mathrm{TE}_{mn}$ modes of the waveguide ($m+n$ modes in total). It is worth noting that, since the modes have an oscillatory behavior, it is reasonable to model them with second-order terms [19], as in the right-hand side of (17).

The roots of $N(z)$ (zeros of $H_d(z)$) are associated with the weights of each mode in the overall response of the system and $n+m=n_a/2$ (since the order of the denominator of $H_d(z)$ is $n_a$ and there are $n+m$ terms in the expansion, each one with a second-order denominator). Each partial fraction describes a propagating mode inside the waveguide. The $i$th mode will have a weight, resonant frequency of oscillation, and damping ratio associated with the roots of the polynomial in the $i$th denominator. It is worth noting that this is the minimal representation needed to describe a mode since the first-order term in the numerator of the partial fraction will account for the cut-on effect in the frequency domain, whereas the second-order term in the denominator will ensure that the response is attenuated at high frequencies. For modeling parsimony, no extra zeros or poles are incorporated in the description of each mode. Parameters $a_i$ and $b_i$ can be obtained by minimizing the mean square value of the residual $\varepsilon[\mathrm{k}]$ over the time horizon used for identification using a least squares procedure.

When choosing the model order $(n_a)$, one must make an assumption on the number of modes that are propagating in the structure. The value of $n_k$ can be accurately estimated after observing the delay in the time-domain signatures recorded by the spectrometer from

$$\varphi(\omega)=\tan^{-1}\left[\mathrm{Im}\big(H(\omega)\big)/\mathrm{Re}\big(H(\omega)\big)\right] \tag{18}$$

where $\varphi(\omega)=z^{-n_k}$ [17]. The choice of $n_b$ can be made in an empirical way from cross-correlation of the outputs with the residuals. Other methods such as spectral analysis, analysis of the information matrix, Akaike's final error prediction criterion, or Akaike's information theoretic criterion [8] are also appropriate. The System Identification Toolbox of MATLAB chooses $n_b$ on the basis of parsimony arguments in order to balance the accuracy and complexity (number of parameters to be identified) of the model.

It is worth noting that the use of physical insight in the identification procedure reduces the number of design choices that need to be done on the basis of the data themselves. If the entire definition of the model structure (including the choice of $n_a$ and $n_k$) were data driven, the identification procedure would be more sensitive to artifacts and noise.

The experimental time-domain reflection signatures from the backshorts must be aligned with respect to each other before an identification model is applied to the discretized time-domain signatures. Using the known dimensions of the rectangular section of the waveguide, the cut-on frequency, guide wavelength, and theoretical phase delay at each frequency for each mode for all $\mathrm{TE}_{mn}$ modes propagating in the structure can be calculated [20]. To calculate the overall phase delay, vectorial addition must be performed for all the propagating modes inside the waveguide. Since each mode is attenuated to a different degree, its contribution must be weighted by a weight $w_i$ and a factor with an attenuation constant $\alpha_i$

$$H(\omega)=\sum_{i=1}^{m+n} w_i\big(e^{-\alpha_i(\omega)d/2}e^{j\varphi_i(\omega)}\big). \tag{19}$$

By matching the theoretical calculations for the phase delay in WR-8 waveguide samples to the recorded delay by the interferometer, it was concluded that most of the power is distributed among two modes and, thus, a fourth-order model should be adopted for the backshort experiment. In addition, an examination of the phase velocity of the received signal shows that the propagation of terahertz pulses inside the waveguide is almost dispersion free within the bandwidth of the excitation pulse. Such preferential coupling of the pulse energy to the lower order modes of the structure and the almost dispersion-free propagation observed are similar to the ones obtained by Grischkowsky's group [21] where they also used broad-band excitation in their experimental procedure to characterize plastic ribbon terahertz waveguides.

### B. State-Space Modeling

An alternative way to obtain $H_d(z)$ would be through a state-space modeling approach. Discrete time state-space models represent difference equations, as ARX models do, but are rearranged such that only one delay is used in the expression. This leads to the introduction of extra variables, known as state variables, which are not measured, but can, under certain conditions, be reconstructed from input–output data. For the waveguide characterization problem, a single-input single-output state space model may be identified directly from the data

$$\begin{aligned}\mathbf{x}[\mathrm{k}+1]&=\mathbf{A}\mathbf{x}[\mathrm{k}]+\mathbf{B}u[\mathrm{k}]+\mathbf{K}e[\mathrm{k}]\\ y[\mathrm{k}]&=\mathbf{C}\mathbf{x}[\mathrm{k}]+Du[\mathrm{k}]+e[\mathrm{k}]\end{aligned} \tag{20}$$

where $\mathbf{x}[\mathrm{k}]$ is an $n$-dimensional state vector, $u[k]$ is a deterministic input, $y[k]$ is the measured output, $e[k]$ is the output residual, $D$ is a scalar parameter, and $\mathbf{A},\mathbf{B},\mathbf{C},$ and $\mathbf{K}$ are matrices of the appropriate dimensions. A sound method for estimating the state-space model parameters using input–output data is the subspace approach [22], [23]. A more detailed description of the subspace algorithm as applied to optical systems is provided elsewhere [24]. A common implementation is the N4SID algorithm, which is available as part of MATLAB's System Identification Toolbox.

There is an equivalence between the state-space representation, and the input–output representation. Taking the $z$-transform of the state-space model and eliminating the state variables, it follows that

$$H_d(z)=\frac{Y(z)}{U(z)}=\mathbf{C}(z\mathbf{I}-\mathbf{A})^{-1}\mathbf{B}+D. \tag{21}$$

Writing both ARX, as well as state-space models in an input/output form, a direct comparison of the two methods is possible. However, the state-space representation can be deemed more appropriate than the ARX representation in optimal estimation and optimal control frameworks, as discussed in [24].

Instead of relying on matching the observed phase delay in the interferometer with theoretical models of phase delay that take into account the waveguide dimensions to define the model order as the ARX model does, the subspace algorithm avoids

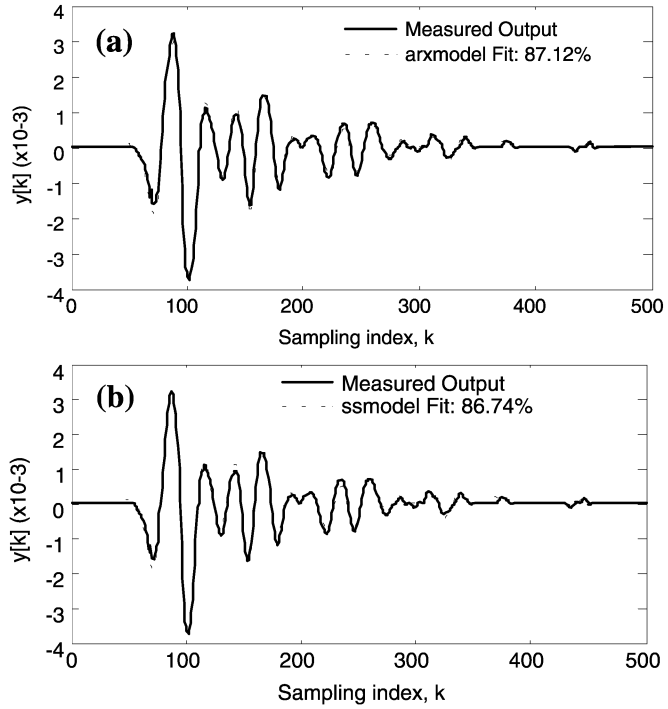


Fig. 5. Measured (solid line) and simulated (dotted line) time-domain responses using the: (a) ARX model and (b) state-space model (modeling data, $d_3/d_2$ case).

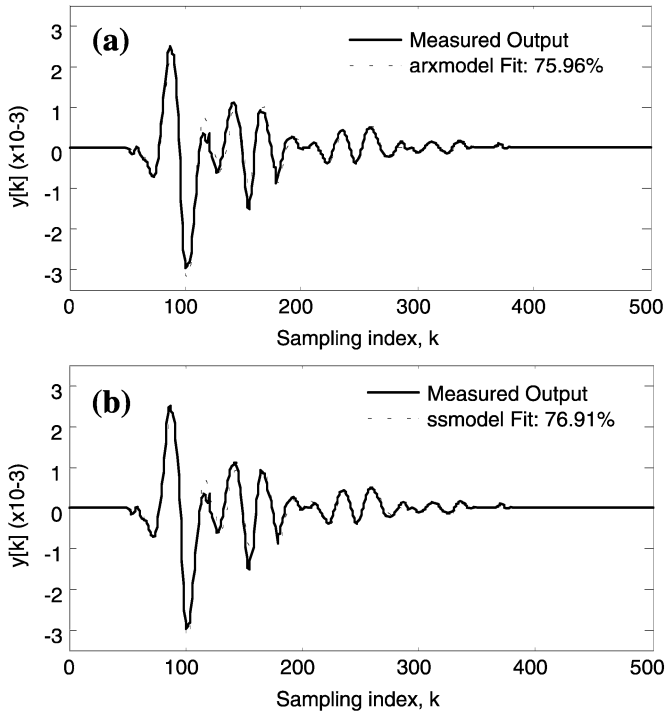


Fig. 6. Measured (solid line) and simulated (dotted line) time-domain responses using the: (a) ARX model and (b) state-space model (validation data, $d_5/d_4$ case).

over-parametrization by observing the singular values plot resulting from the singular value decomposition of a Hankel matrix built from the input–output data [22]. The optimal model order is selected in such a way that the singular values for higher orders are comparatively smaller.

## V. Results and Discussion

The System Identification Toolbox of MATLAB v.6.1 was used to obtain models in the form of (17) and (21). Fig. 5 compares the measured and simulated time domain responses for the modeling data, which consisted of the signals for two- and three-waveguide-length units. Both the ARX and state-space models reproduced 87% of the $y$-variance.

Readers familiarized with control systems theory will notice that the time-domain plots of Fig. 5 resemble impulse responses of nonminimum phase systems [19]. However, one should bear in mind that those are the responses of the entire structure (including the coupling of the test piece), whereas the models considered in this paper are developed for the waveguide only (the coupling effects being ratioed out). Thus, if the nonminimum phase behavior is actually caused by coupling effects, it should not be reflected in the identified models.

For validation, the models were applied to an independent data set consisting of the responses for four- and five-waveguide-length units. The results presented in Fig. 6 show that the model predictions are in good agreement with the measured responses. It is worth noting that the accuracy is smaller in the validation set, as compared to the modeling set (Fig. 5). Such a finding was to be expected because the validation data are not included in the model-building process. They are used instead to check the generalization ability of the model, i.e., its ability to predict the behavior of the system in a situation that is not exactly equal to the one considered in the modeling phase [8].

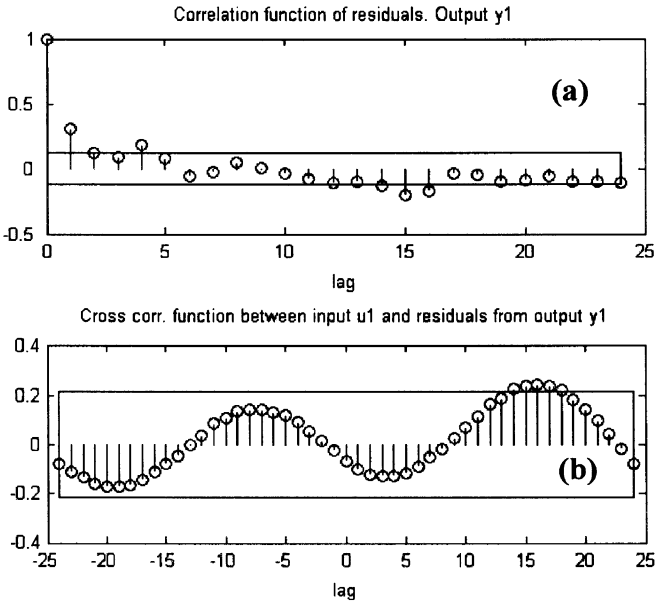


Fig. 7. Residual statistics for the state-space model with the $d_5/d_4$ validation data. (a) Autocorrelation values of the modeling residual $e[\mathrm{k}]$. (b) Cross-correlation between the modeling residual and input signal.

Fig. 7(a) shows the autocorrelation values of the state space model residual $\sum_{\mathrm{k}} e[\mathrm{k}]e[\mathrm{k}-p]$, where $p$ is a time lag between two points of the state-space model residual sequence. Fig. 7(b) shows the cross-correlation $\sum_{\mathrm{k}} e[\mathrm{k}]u[\mathrm{k}-p]$ between the modeling residual and input signal for different time lags $p$.

Fig. 8(a) and (b) shows similar residual correlation plots for the ARX model. Ideally, the autocorrelation should be zero for

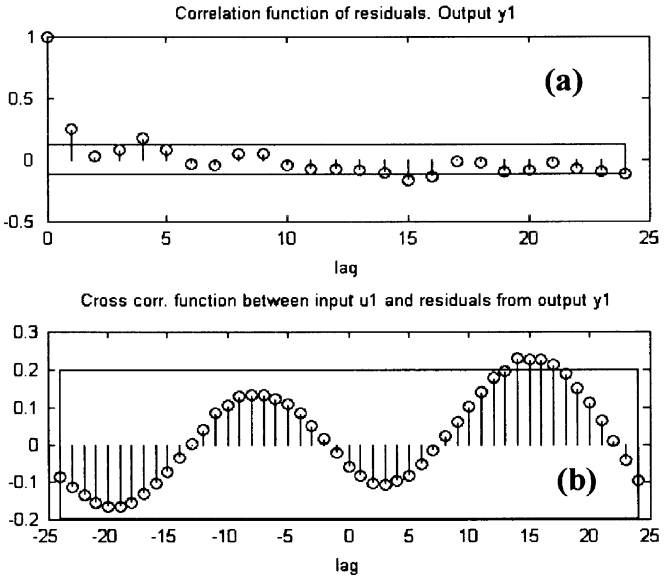


Fig. 8. Residual statistics for the ARX model and the $d_5/d_4$ validation data. (a) Autocorrelation values of the modeling residual $\varepsilon[k]$. (b) Cross-correlation between the modeling residual and input signal.

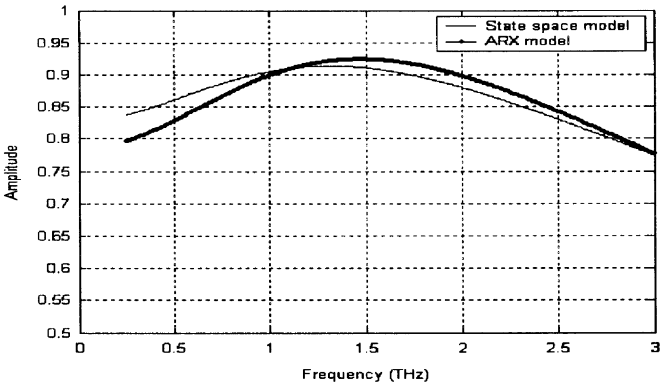


Fig. 9. Calculated transmission coefficient $|H(jw)|$ of a unit length waveguide for the backshort.

time lags different from zero (white noise) and there should be no cross-correlation between the residual and input since any correlation would indicate that part of the residual could be predicted from the input. Since the autocorrelation of the residuals is small, the assumption of whiteness in the noise can be assumed to be valid.

Fig. 9 shows the insertion loss of a unit length waveguide (as calculated both by the ARX and state-space models) after ratioing the spectra obtained with the backshort adjusted to 3 mm with that at 2 mm (denoted as the $d_3/d_2$ case), which is, in fact, the frequency response of the identified models. An effective propagation constant for the multimode propagation can, therefore, be calculated [17]. The observed increased insertion loss at higher frequencies is attributed to the variation of the conductivity of gold with frequency.

The pole-zero charts in Figs. 10 and 11 provide details of the resulting ARX model and state-space model (when converted to an input–output model). The dashed isoclines provide values of

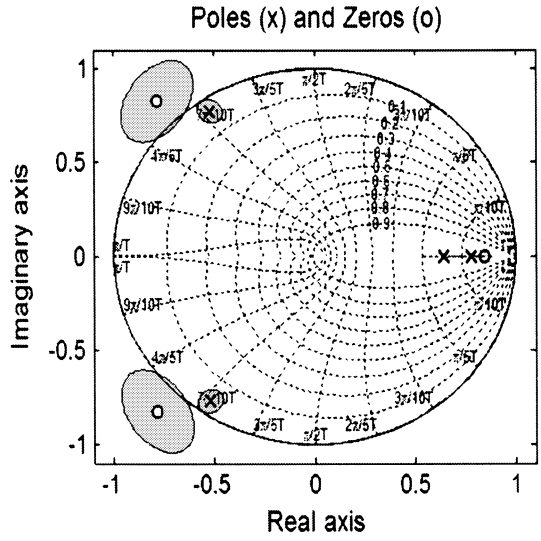


Fig. 10. Pole-zero diagram for the state-space model showing the confidence regions using one standard deviation.

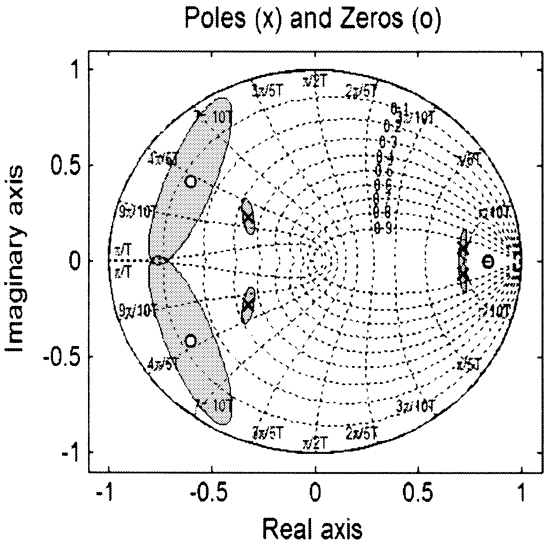


Fig. 11. Pole-zero diagram for the ARX model showing the confidence regions using one standard deviation.

natural frequencies $\omega_n$ and damping ratios $\zeta$ for the propagating modes. The isoclines are obtained from

$$z = \exp\left[T_s(-\zeta\omega_n \pm j\omega_n\sqrt{(1-\zeta^2)}\right] \tag{22}$$

where $0 \le \zeta \le 1, \omega_n \ge 0$ by fixing $\zeta$ and varying $\omega_n$ or by fixing $\omega_n$ and varying $\zeta$.

In these plots, the confidence locus of the zeros is much larger than the confidence locus of the poles. This was to be expected since it is easier to estimate poles than zeros, as they are associated with the exponential decay and frequency of oscillation of the modes, whereas the zeros are associated with the weights of each mode, which are intuitively more difficult to obtain. In addition, if more modes were assumed in the model, the radii of the confidence zones of the poles and zeros would increase since the number of unknowns would be larger for the same number of observations, i.e., the confidence levels in the model decrease significantly when the model is over-parametrized.

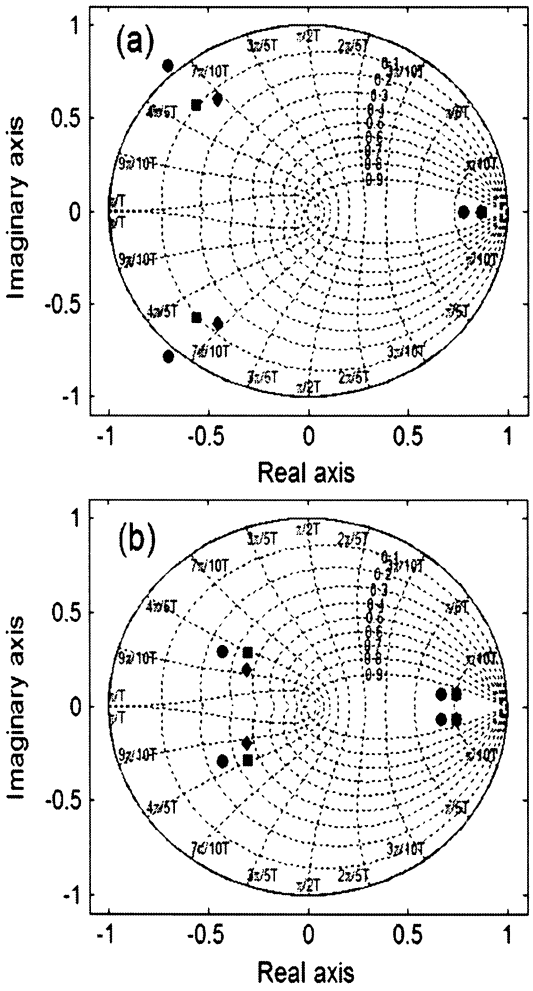


Fig. 12. (a) Zero- and (b) pole-charts of original (•), wavelet-filtered (■), optimal wavelet-filtered (◇) responses assuming a fourth-order ARX model.

Since the autocorrelation function of the residual for both the ARX and state-space models is almost within the one standard error bounds, it can be concluded that the models have been appropriately chosen. Some of the zeros calculated using the state-space model are outside the unit circle, which indicates that this model exhibits nonminimum phase behavior, which is not the case with the identified ARX model.

Fig. 12 provides pole and zero charts where an ARX identification model is used to obtain $H_d(z)$ after assuming two modes propagating in the structure. It was observed that the wavelet filtering process resulted in a zero that was outside the unit circle being brought to the inside. This is in accordance with our expectations since there does not seem to be a physical reason for a zero being outside the unit circle.

As stated earlier, the poles are directly related to the mode properties. Filtering increased the estimated damping in the higher frequency mode. The frequency itself remained practically unchanged. Furthermore, in the lower frequency mode, the filtering decreased the estimated frequency, whereas the damping remained unchanged.

A premise of this study is that the filtering procedure improves the signal-to-noise ratio of the measurements and, consequently, the accuracy of the identification results. However, one should bear in mind that if the filtering is too aggressive (in the sense of more wavelet coefficients being replaced with zeros), there is a risk that the identified model will be related to the filter dynamics rather than to the waveguide response. At this point, it is worth noting that the proposed wavelet optimization procedure may actually alleviate such a risk. In fact, by tailoring the wavelet transform to the denoising task, it is possible to minimize the distortion effects on the signal caused by removing the noise.

## VI. Conclusion

Both ARX and state-space models are efficient modeling tools for linear processes such as energy dissipation in a waveguide test piece. These tools, however, require low-noise data sets, which might not be realizable within practical integration time scales. Wavelet pre-filtering is well suited to the denoising of the nonstationary data sets obtained in terahertz transient spectrometry.

One limitation of commonly used wavelets such as the $db4$ family is that the wavelets must be chosen *a priori* and are not adapted to optimally describe the experimental data set. We, therefore, introduced a QMF bank to optimize the compression ability of the transform before performing any thresholding in the wavelet domain. The optimal filtering procedure employed in this study was aimed at maximizing the amount of energy in the wavelet coefficients kept in the thresholding process.

Although pre-filtering of the time-domain signatures with a $db4$ and an optimal filter did not produce traces that would be classified as different by eye inspection, these different filtering procedures had a marked effect on the pole-zero diagrams obtained after ARX and subspace models were fitted to the data. This justifies their use in waveguide mode identification from broad-band experiments.

An extension of the subspace algorithm to bilinear systems would be required to take into account the nonlinearities of the cut-on conditions in the modes and account for evanescent fields for a more accurate model. In this case, the complex values arising in the simulations would be treated separately in matrix form in a similar manner to real valued data. The good fit, however, of both models to the time-domain data sets indicated that this was not necessary in our current analysis. In fact, since the scope of this study was restricted to the modeling of the propagating modes, the cut-on conditions and the evanescent fields were not modeled or considered in the validation of the obtained models. Different experimental protocols may be designed to focus the study on such a phenomena. In that case, the nonlinear effects would have to be properly taken into account.

Finally, it is worth noting that, although the proposed analysis in the wavelet domain has been placed within a filtering framework, there have been suggestions [25] that such transforms may also be used directly for waveguide mode identification.

## References

[1] D. M. Mittleman, G. Gupta, R. Neelamani, R. G. Baraniuk, J. V. Rudd, and M. Koch, "Recent advances in terahertz imaging," *Appl. Phys. B, Photophys. Laser Chem.*, vol. 68, pp. 1085–1094, 1999.

[2] D. M. Mittleman, R. H. Jacobsen, R. Neelamani, R. G. Baraniuk, and M. C. Nuss, "Gas sensing using terahertz time-domain spectroscopy," *Appl. Phys. B, Photophys. Laser Chem.*, vol. 67, pp. 379–390, 1998.

[3] B. Ferguson and D. Abbott, "Wavelet de-noising of optical terahertz imaging data," *Fluctuation Noise Lett.*, vol. 1, pp. L65–L70, 2001.

[4] P. R. Smith, D. H. Auston, and M. C. Nuss, "Subpicosecond photoconducting dipole antennas," *J. Quantum Electron*, vol. QE-24, pp. 255–260, Feb. 1988.
[5] M. C. Nuss and J. Orenstein, "Millimeter and submillimeter wave spectroscopy of solids," in *Topics Current Chem.*, E. Grüner, Ed. Heidelberg, Germany: Springer-Verlag, 1998, vol. 74, pp. 7–50.
[6] P. Haring-Bolívar, "Coherent THz spectroscopy," in *Semiconductor Quantum Optoelectronics: From Quantum Physics to Smart Devices*, A. Miller, M. Ebrahimzahdeh, and D. M. Finlayson, Eds. Bristol, U.K.: Institute of Phys., 1999, ch. 5, pp. 151–192.
[7] P. Haring-Bolívar, M. Brucherseifer, H. P. M. Pellemans, and H. Kurz *et al.*, "THz sources and systems," in *Time Domain THz Spectroscopy and Sensing*, R. E. Miles *et al.*, Eds. Norwell, MA: Kluwer, 2001, pp. 315–328.
[8] L. Ljung, *System Identification, Theory for the User*, 2nd ed. Upper Saddle River, NJ: Prentice-Hall, 1999.
[9] H. Krim, D. Tucker, S. G. Mallat, and D. Donoho, "On denoising and best signal representation," *IEEE Trans. Inform. Theory*, vol. 45, pp. 2225–2238, Nov. 1999.
[10] U. L. Pen, "Application of wavelets to filtering of noisy data," *Phil. Trans. R. Soc. Lond. A, Math. Phys. Eng. Sci.*, vol. 357, pp. 2561–2571, Sept. 1999.
[11] G. Strang and T. Nguyen, *Wavelets and Filter Banks*, rev. ed. Wellesley, MA: Wellesley-Cambridge, 1998.
[12] P. P. Vaidyanathan, *Multirate Systems and Filter Banks*. Englewood Cliffs, NJ: Prentice-Hall, 1993.
[13] B. G. Sherlock and D. M. Monro, "On the space of orthonormal wavelets," *IEEE Trans. Signal Processing*, vol. 46, pp. 1716–1720, June 1998.
[14] I. Daubechies, *Ten Lectures on Wavelets*, ser. CBMS-NSF Appl. Math. 61. Philadelphia, PA: SIAM, 1992.
[15] J. Tuqun and P. P. Vaidyanathan, "A state-space approach to the design of globally optimal FIR energy compaction filters," *IEEE Trans. Signal Processing*, vol. 48, pp. 2822–2838, Oct. 2000.
[16] M. Misiti, Y. Misiti, G. Oppenheim, and J. M. Poggi, *Wavelet Toolbox User's Guide*. Natick, MA: The Mathworks, 1996.
[17] S. Hadjiloucas, R. K. H. Galvão, J. W. Bowen, R. Martini, M. Brucherseifer, H. P. M. Pellemans, P. Haring-Bolívar, H. Kurz, J. Digby, G. M. Parkhurst, and J. M. Chamberlain, "Measurement of propagation constant in waveguides using wideband coherent THz spectroscopy," *J. Opt. Soc. Amer. B, Opt. Phys.*, vol. 20, pp. 391–401, Feb. 2003.
[18] S. M. Kay and S. L. Marple, Jr., "Spectrum analysis: A modern perspective," *Proc. IEEE*, vol. 69, pp. 1380–1419, Nov. 1981.
[19] B. C. Kuo, *Automatic Control Systems*, 7th ed. Englewood Cliffs, NJ: Prentice-Hall, 1995.
[20] *Waveguide Handbook*, Peregrinus, London, U.K., 1993. N. Marcuvitz.
[21] R. Mendis and D. Grischkowsky, "Plastic ribbon THz waveguides," *J. Appl. Phys.*, vol. 88, pp. 4449–4451, Oct. 2000.
[22] P. Van Overschee and B. DeMoor, "N4SID: Subspace algorithms for the identification of combined deterministic-stochastic systems," *Automatica*, vol. 30, pp. 75–93, Jan. 1994.
[23] M. Verhaegen, "Identification of the deterministic part of MIMO state space models, given in innovations form from input–output data," *Automatica*, vol. 30, pp. 61–74, Jan. 1994.
[24] R. K. H. Galvão, S. Hadjiloucas, V. M. Becerra, and J. W. Bowen, "Subspace systems identification framework for the analysis of multimoded propagation of THz-transient signals," unpublished.
[25] J. C. Goswami, K. Chan, and C. K. Chui, "An application of fast integral wavelet transform to waveguide mode identification," *IEEE Trans. Microwave Theory Tech.*, vol. 43, pp. 655–663, Mar. 1995.

**Sillas Hadjiloucas** (M'94) was born in Athens Greece, in 1966. He received the B.Sc. (with honors) and M.Phil. degrees in pure and applied biology from The University of Leeds, Leeds, U.K., in 1989 and 1992, respectively, and the Ph.D. degree in cybernetics from The University of Reading, Reading, U.K., in 1996.

Upon serving with the Greek Army in 1997, he held two appointments as an European Community (EC) Training and Mobility of Researchers (TMR) Post-Doctoral Research Fellow involved with terahertz instrumentation as part of the International Terahertz Action (INTERACT) Project in Reading, U.K., and the Deutschen Zentrum für Luft- und Raumfahrt (DLR) Berlin, Berlin, Germany. Since January 2000, he has been a Lecturer with the Department of Cybernetics, The University of Reading. His scientific interests are directed toward the development of instrumentation and feedback measurement techniques in the optical, infrared, far-infrared, millimeter-wave, and microwave parts of the spectrum with applications to biology. He teaches the Advanced Instrumentation and Biomedical Instrumentation modules for M.Sc. students in cybernetics. He is currently also involved in the setup of the Ultrafast Laser Laboratory, The University of Reading, as well as with the application of control theory and system identification techniques to optical systems and spectroscopy.

Dr. Hadjiloucas is a member of the Institute of Biology (MIBiol CBiol), the Institute of Physics (MInstP, CPhys), the European Optical Society (EOS), and Optical Society of America (OSA).

**Roberto K. H. Galvão** received the B.Sc. degree (*summa cum laude*) in electronics engineering and Ph.D. degree in systems and control from the Instituto Tecnológico de Aeronáutica (ITA), São José dos Campos, São Paulo, Brazil, in 1995 and 1999, respectively.

In 2001, he spent a post-doctoral period with the Cybernetics Department, The University of Reading, Reading, UK. Since 1998, he has been an Associate Professor of systems and control with the Divisão de Engenharia Eletrônica, ITA. His main areas of interest are wavelet theory and applications, system identification, and multivariate analysis.

**Victor M. Becerra** (S'91–M'95–SM'03) received the B.Sc. degree (*cum laude*) in electrical engineering from Simon Bolivar University, Caracas, Venezuela, in 1990, the Ph.D. degree in control engineering from City University, London, U.K., in 1994, and the M.Sc. degree in financial management from Middlesex University, London, U.K., in 2001.

From 1989 to 1991, he was with Corporación Venezolana de Guayana (C. V. G.) Edelca, Caracas, Venezuela, where he was involved with power systems analysis and control. From 1994 to 1999, he was a Research Fellow in control systems with City University, London, U.K. Since January 2000, he has been a Lecturer with the Department of Cybernetics, The University of Reading, Reading, U.K., where he lectures in the field of control engineering. His main research interest is in the areas of control systems and its intersections with artificial intelligence. He is the head of the Cybernetics Intelligence Research Group, The University of Reading.

Dr. Becerra is a member of the Institution of Electrical Engineers (IEE), U.K.

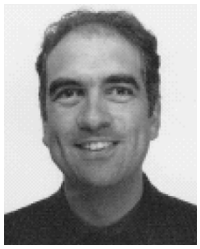

**John W. Bowen** was born in Malvern, Worcestershire, U.K., in 1963. He received the degree in physics from Queen Mary College, University of London, London, U.K., in 1985, and the Ph.D. degree from the University of London, London, U.K., in 1993. His doctoral research concerned techniques for wide-band millimeter-wave spectrometry.

He was a consultant for QMC Instruments Ltd., and as a Research Associate with Queen Mary College and Westfield College, University of London, U.K. In 1993, he joined the Department of Cybernetics, The University of Reading, Reading, U.K., as a Lecturer. He is currently Head of the Department of Cybernetics and Senior Lecturer in cybernetics. He also heads the Instrumentation and Signal Processing Research Group. His research interests include millimeter-wave and terahertz optical systems design, millimeter-wave and terahertz spectrometry, the interaction of terahertz radiation with biological tissue at both the macroscopic and cellular levels, terahertz imaging and signal processing, solid-state noise sources, and wide-band antennas.

Dr. Bowen was the recipient of the 1989 U.K. National Physical Laboratory Metrology Award for his suggestion for a new wide-band solid-state noise source for millimeter-wave spectrometry.

**Rainer Martini**, photograph and biography not available at time of publication.

**Martin Brucherseifer** was born on May 16, 1967, in Wissen, Germany. He received the Diploma and Doctor degrees in electrical engineering from the Rheinisch-Westfälische Technische Hochschule (RWTH), Aachen, Germany, in 1997 and 2002, respectively.

He is currently with the Georgia Institute of Technology, Atlanta, where he is involved with the combination of scanning probe microscopy with infrared (IR) spectroscopy. His research has comprised highly sensitive and spatially resolved terahertz spectroscopy. He was involved with free-space telecommunication in the far infrared and terahertz frequency range with the Department of Physics and Engineering Physics, Stevens Institute of Technology, Hoboken, NJ.

**Harm P. M. Pellemans**, photograph and biography not available at time of publication.

**Peter Haring Bolívar** (M'02) was born in Mexico City, Mexico, in 1969. He received degrees from the Rheinisch-Westfälische Technische Hochschule (RWTH) Aachen University, Aachen, Germany.

From 1992 to 1993, he was Head of the Rescue Equipment Division, Nautica Diesel Europea, Mexico City, Mexico. From 1993 to 1996, he was a Scientific Assistant with the Institut für Halbleitertechnik, RWTH Aachen, where he was involved with conjugated polymers and femtosecond dynamics in semiconductors. From 1997 to 2001, he was Head of ultrahigh-frequency research with the Institut of Semiconductor Electronics, RWTH Aachen, where he directed applied and fundamental scientific research on coherent terahertz spectroscopy and ultrahigh-frequency optical characterization of electronic gigahertz devices. Since 2001, he is Head of research (it Oberingenieur) at RWTH Aachen, where he is involved with activities in the fields of opto-electronics, ultrafast science, ultrahigh-frequency devices, optical data storage, and nanotechnology. He has authored or coauthored five book contributions and over 130 publications and international conference presentations. He holds three patents.

Dr. Bolívar was the recipient of a Heinrich Hertz Fellowship from the Science and Research Ministry of the State of Northrhine–Westfalia for his doctoral research. He was also the recipient of the Wilhelm Borchers Medallion of RWTH Aachen.

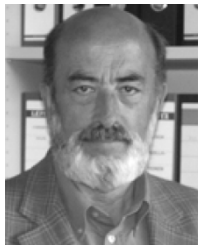

**Heinrich Kurz** was born in Austria, in 1943. He received the Ph.D. degree from the University of Vienna, Vienna, Austria, in 1971.

From 1971 to 1980, he was Scientific Staff Member with Philips Research Laboratories, Hamburg, Germany, where he was engaged in research on optical storage and data processing. From 1981 to 1984, he was with a Research Associate with Harvard University, during which time his scientific interest was directed toward the interaction of ultrashort laser pulses with semiconductors. Since 1985, he has been a Professor of electric engineering with the Rheinisch-Westfälische Technische Hochschule (RWTH), Aachen, Germany. His research includes nonlinear optics, femtosecond laser interactions, and spectroscopy and application of ultrashort laser pulses in electrical engineering and material science. Since 1990, he has been the Head of the Institut für Halbleitertechnik, RWTH Aachen, taking the Chair of Semiconductor Electronics. His main research activities have been extended to nanoelectronics, mainly silicon-based nanoelectronics and nanotechnology in general for information science. In 1993, he founded the AMO GmbH, a nonprofit organization, to promote science and technology from university research into strategic industrial areas. Since 1997, he is the Scientific Director of the Advanced Microelectronic Center Aachen (AMICA) built by the AMO GmbH. Since 1998, he coordinates the national efforts in Germany on nanoelectronics and functional lateral nanostructures in general.

**J. Martyn Chamberlain** has been involved with issues related to the applicable physics of the terahertz-frequency regime for over 30 years. His graduate work at Oxford University centered on terahertz-frequency investigations of the electrical properties of ultra-pure III–V semiconductors using techniques which, at the time, were extremely novel. He subsequently joined Nottingham University, Nottingham, U.K., as a Lecturer in physics. Into the 1980s, he assumed control of the semiconductor characterization facility at Nottingham University, which was part of a very substantial investment in semiconductor physics that was initiated at that time in the U.K. In 1989, he was appointed Reader in experimental physics at Nottingham University. During that time, his interests were in the development of small solid-state devices as potential sources of terahertz radiation. These included resonant tunnel diodes, superlattice oscillators, self-oscillating mixers, and other devices. In addition, he also pioneered micromachining techniques to realize passive terahertz frequency circuits that contained such active devices. In 1999, he joined The University of Leeds, as Professor of engineering physics and Director of the Institute for Microwaves and Photonics. He continued research on solid-state sources for terahertz use and on systems for the optical generation of pulses of terahertz radiation. This led to a large European Project (Teravision), which he coordinated, and for which he was dedicated to the realization of practical terahertz systems for potential use in medical diagnostics. Since September 2003, he has held a dual appointment as Master (i.e., President) of Grey College, University of Durham, Durham, U.K., and Professor of applied physics with the University of Durham. In September 2004, he will become Coordinator of the multimillion European Union program TeraNova, which brings together academic and industrial groups in Europe working on new terahertz sources and systems for use in healthcare, biotechnology, security, and process control. He has authored or coauthored approximately 200 refereed papers and has presented numerous invited talks and summer schools. He acts as consultant to a number of companies, and sits on several U.K. government panels.

Dr. Chamberlain has organized numerous conferences, including the First International Conference on Biomedical Imaging and Sensing Applications of Terahertz Technology, held in the U.K. in 2001.